Aluminium-Rubber Composite - Experimental and Numerical Analysis of Perforation Process at Ambient and High Temperatures

M. Klosak[a*], A. Bendarma[a,b], T. Jankowiak[b], S. Bahi[c], A. Rusinek[c]

[a] Universiapolis, Technical University of Agadir, Laboratory for Sustainable Innovation and Applied Research, Bab Al Madina, BP 8143, Qr Tilila, 80000 Agadir, Morocco; E-mail: klosak@e-polytechnique.ma, b.amine@e-polytechnique.ma

[b] Poznan University of Technology, Institute of Structural Analysis, Piotrowo 5, 60-965, Poznan, Poland; E-mail: tomasz.jankowiak@put.poznan.pl

[c] University of Lorraine, Laboratory of Microstructure Studies and Mechanics of Materials LEM3, 7 Rue Félix Savart, 57070 Metz, France; E-mail: mohamed-slim.bahi@univ-lorraine.fr, alexis.rusinek@univ-lorraine.fr

Abstract: In this work, the impact resistance of an aluminium–rubber sandwich composite plate under impact loading is investigated using experimental and numerical approaches. The experimental tests were carried out using a perforation gas gun for a wide range of impact velocities from 40 m/s to 120 m/s and for two different temperatures 20°C and 150°C. Based on experimental results, the failure mode, initial/residual velocity curves and the ballistic limit velocities of aluminium under different temperatures were analysed. The effect of rubber reinforcement layer thickness in the aluminium sandwich was also evaluated. It was found that the composite plate with 9 mm of rubber provides higher performance in terms of energy absorption than that of 3 mm thick, which is demonstrated by approximately 10% reduction in the ballistic limit. In contrast, an increase in temperature considerably reduces these ballistic performances. It was also found that petaling is a typical failure mode in the perforation process. The rubber has an effect on the failure pattern of both aluminum plates. In addition, a thermomechanical model using a finite element method was developed to simulate the response of the aluminum–rubber composite plate under a high energy rate loading condition. The numerical results show a good agreement in relation to the experimental results in terms of failure mechanism, number of petals and energy absorption.

Keywords: aluminium-rubber sandwich panel; pneumatic gas gun; high strain rates

1 Introduction

For many years, the perforation capability of armor plates made of aluminum alloys has been studied due to their good formability, low-density, and high impact performance. The recent studies have been proposed in order to investigate the ballistic performance of aluminum plates under impact of projectile through experimental and numerical approaches [1-5]. Alavi Nia and Hoseini [6] compared ballistic resistance performance of monolithic, in-contact layered and spaced layered aluminum plates. They found that under the same total target thickness, the monolithic target behaved in the most optimal way, followed by an in-contact layered target and a spaced layered target. Moreover, with a specially designed drop weight tower, low velocity impact behavior of AA 2024-T3 aluminum at -60° C was investigated by Martínez et al. [7]. It was observed that the target absorbed a larger impact energy with decreasing temperature, and the improved protection performance at low temperature came from temperature sensitivity of the material.

In order to investigate perforation behavior of materials at elevated temperatures, Rusinek et al. [8] proposed a heating chamber coupled with a ballistic impact device. With the thermal chamber, Klosak et al. [9] studied perforation behaviour of brass alloy plates under temperatures ranging from 20° C to 260° C. Results showed that the energy absorption capacity decreased with increasing temperature: the absorbed energy changed from 31.2 J at room temperature to 20.9 J at 260° C. Bin et al. [10], studied the deformation behaviour of 304 austenite stainless steel under dynamic loading from -165° C to 260° C. It was shown that the ballistic limit velocity V_B is sensitive to the testing temperature. It increases slightly from 93 m/s at 200° C to 103 m/s at -20° C and then remains constant at still lower temperatures. The material shows better energy absorption capacity at low temperatures. The improved ballistic resistance performance at low temperatures comes from not only temperature sensitivity of the material but also its Strain-Induced Martensitic Transformation (SIMT) effect.

In the last decades, many researchers have focused on performance improvement of structural protections against impact threats [11-13] by including a hyperelastic material as a shock absorber. These different studies concluded that the use of hyperelastic reinforcement in composite structures decreases the damage due to blast load and penetration of projectile with higher dissipation of kinetic energy under impact loadings.

One of the widely used materials exploited as a shock absorber reinforcement is the natural rubber, which is characterized by a higher impact resistance, high level of damping properties and flexibility, and an excellent puncture and tear resistance [14-20]. In fact, a proper composite structure should keep a balance between strength and ductility which are opposite material features.

The purpose of this study, therefore, is to study the effect of temperature on perforation behaviour of the sandwich structure aluminium-rubber using a gas gun setup. First, the effect of rubber thickness on the energy of absorption, reaction force is presented at room temperature. The initial temperature effect on the ballistic performance is discussed for tests carried out under room temperature and at 150° C. The experimental setup helps measure the initial velocity and residual velocity curves of the material in order to determine the Ipson and Recht model coefficients [21]. The failure pattern, initial and residual velocity curves and absorbed energy of the reinforced structure at two different temperatures were compared to numerical model results and then discussed.

2 Experimental Set-up

The dynamic study was carried out using a pneumatic gas gun, whose scheme and photo are presented in Fig. 1. A wide range of impact velocities from 40 m/s to 120 m/s has been covered during the perforation tests.

The projectile with a conical shape is launched through a tube using a pneumatic gas gun. At the end of the gun barrel, two laser sensors are mounted to measure the initial velocity of the projectile V_0. This can later be obtained by dividing the distance Δd between two sensors by the time $\Delta t = t1 - t2$, needed for the projectile to cover the distance between them. Based on the same measurement method, the residual velocity V_R is measured after the perforation process. The impact velocity V_0 of the projectile is controlled by changing the initial gas gun pressure P_0.

The apparatus is equipped with a thermal chamber in which a specimen is heated. This system which deals with impact loading at elevated temperatures is still not very common in experimental practice, the standard gas gun is usually not coupled with a heating tool. The usual approach is to carry out perforation tests at room temperature and to extrapolate results using numerical simulations at higher temperatures by applying the defined constitutive relation. A detailed description of the thermal chamber is given in [8, 9] and will not be discussed here, the extended experimental analysis using this set-up can be found in [8-10, 22-27].

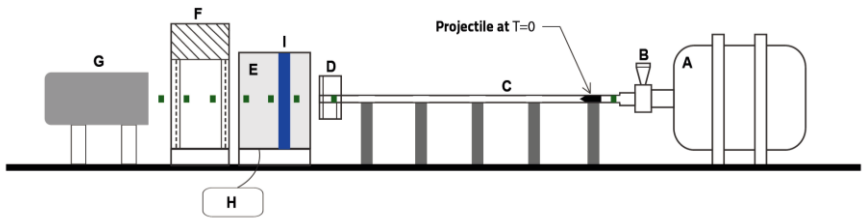

a)

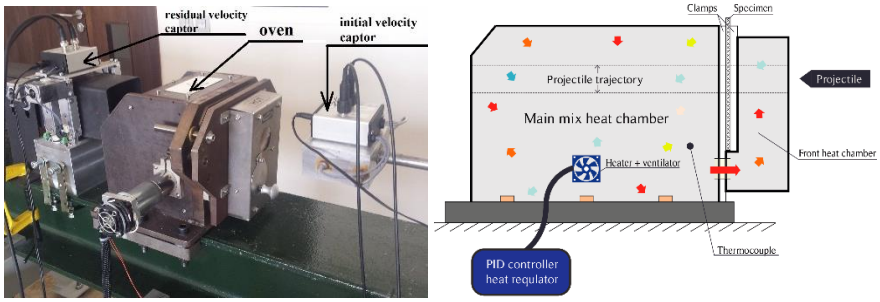

b)

Figure 1

Apparatus for high temperature perforation testing: (a) general view of the ballistic impact device (photo and scheme), (b) thermal chamber (photo and schematic view) [9]

For the measurement of the perforation force, the ballistic impact device is equipped with four piezoelectric sensors fixed on the four corners of the rigid target holder, Fig. 2. A single sensor can undertake a maximum of 20 kN, which makes up a 4-sensor set-up maximum equal to 80 kN.

During the perforation process, part of the kinetic energy of the projectile is absorbed by the sandwich structure. Once the initial V_0 and the residual V_R velocities of the projectile are determined, the energy absorbed by the structure $W_{\text{structure}}$ can be calculated as follows:

$$W_{\text{structure}} = ½\, M_p\, (V_0^2 - V_R^2) \tag{1}$$

where M_p is the mass of the projectile. A part of the kinetic energy, Eq. 1, is transferred to the structure during the process of impact or perforation.

As discussed in [10], the energy lost due to the elastic deformation of the sandwich structure, friction between the projectile and the target as well as that transferred to the ejected debris can be neglected. Then, the energy balance absorbed by the structure can be described as follows:

$$W_{\text{structure}} = W_{pb} + W_{ps} + W_p + W_c \tag{2}$$

where W_{pb} is the plastic bending energy of the sandwich structure, W_{ps} is the plastic stretching energy of the target, W_p is the plastic bending energy of the petals and W_c is the energy dissipation during crack formation and propagation processes.

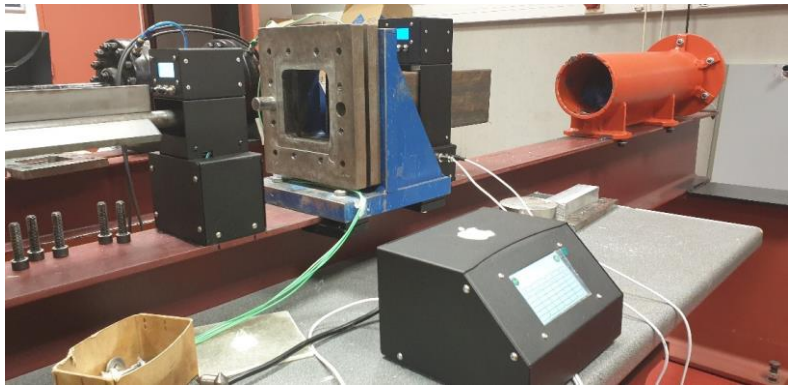

Figure 2
Ballistic impact device equipped with compressive force measurement sensors

The plate-projectile configuration is presented in Fig. 3. The cylindrical projectile with a conical nose has a 72° conical edge, 11.5 mm in diameter and 35 mm in length; its weight is 28 g. The plate specimens are 130 mm x 130 mm and are fully clamped along their perimeter by two rigid metallic rigs, placed in both sides of the plates. The aluminium specimens are made of the alloy with the following chemical composition: Al 99,40% and Fe 0.6%, the material can be considered pure aluminium. Their thickness is 1.0 mm, whereas the rubber element is 3 mm thick. Three configurations of the aluminium-rubber composite were studied and

they are presented in Fig. 4. It is to be noted that no glue was applied between metallic plates and rubber. The 9 mm rubber specimen was composed of three identical pieces of rubber put together with no gluing, either.

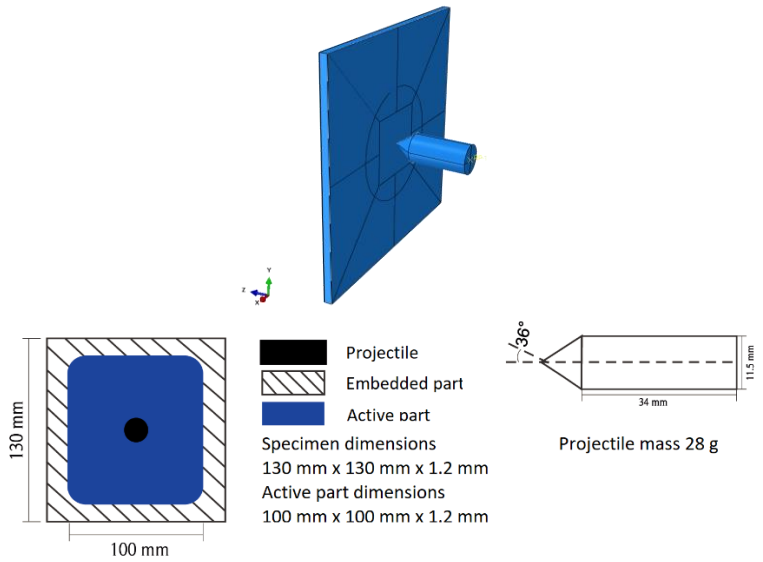

Figure 3

Configuration of plate and cylindrical projectile with a conical nose for the laboratory experiments

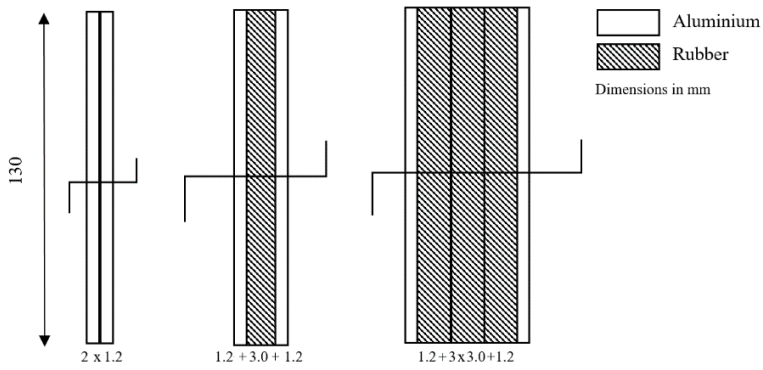

Figure 4

Three configurations of the analysed composite (dimensions in mm), a) no rubber sheet (aluminium plates only), b) aluminium + 1 rubber sheet (3 mm), c) aluminium + 3 rubber sheets (9 mm); no glue beteween sheets

3 Perforation Testing and Ballistic Properties Definition

Perforation tests were carried out with the protocol widely used in literature taking into account the interesting analyses found in [28-32] in which the petaling as a typical failure mode in perforation of the metal plates by a conical projectile is highlighted. The experimental results are collected in Table 1. For each test the laser sensors enabled calculation of the initial and residual velocities. The initial temperatures considered were T_0=293 K, 353 K, 423 K. The determined ballistic limits are presented later in the next section for a comparison with numerical simulations.

The typical petaling is observed in metal plates, although its shape is different for each aluminium plate, which can be seen in Fig. 5. The outer plate develops shapely petals whose observed number is 3 to 4, whereas the inner plate has rather a rugged form with 5-8 irregular petals. The rubber part is torn along one or two lines, experiencing large deformations during the projectile pass, but as the material is hyperelastic, only a small permanent deformation occurs in the vicinity of the perforation.

As may be defined from Table 1, the rubber has an effect on the ballistic limit. The estimated ballistic value increased from 76 m/s to 93 m/s (+22%) for room temperature and from 63 m/s to 74 m/s (+17%) at T_0=423 K when 9 mm rubber layer was added to the sandwich specimen. It confirms that a rubber plate acts as an efficient shock absorber. As the mechanical performances of rubber are by far worse than those of aluminium, this effect can be described as considerable.

Figure 5

Aluminum-rubber composite, from the left: outer aluminium plate, rubber, inner aluminium plate (the inner plate is impacted first by projectile); testing initial conditions: V_0=121.47 m/s, T_0=353 K

Table 1
Experimental data

Aluminium plates only (2x1.0 mm)											
Press. (bars)	**Test No**	**T_0 [K]**	**V_0 (m/s)**	**t (ms)**	**V_R (m/s)**	**Press. (bars)**	**Test No**	**T_0 [K]**	**V_0 (m/s)**	**t (ms)**	**V_R (m/s)**
2.5	31*	293	71.84	0.000	0.00	2.0	41A	423	65.10	4.240	11.79
3.0	32	293	77.88	1.600	31.25	2.5	41	423	73.53	1.320	37.88
4.0	33	293	90.58	0.860	58.14	3.0	42	423	80.91	0.940	53.19
5.0	34	293	100.40	0.700	71.43	4.0	43	423	91.91	0.660	75.76
7.5	35	293	120.77	0.510	98.04	5.0	44	423	100.89	0.560	89.29
						7.5	45	423	120.12	0.470	106.38
Ballistic limit estimation **76 m/s** * projectile stuck						Ballistic limit estimation **63 m/s**					
Aluminium plates + 3 mm rubber											
Press. (bars)	**Test No**	**T_0 [K]**	**V_0 (m/s)**	**t (ms)**	**V_R (m/s)**	**Press. (bars)**	**Test No**	**T_0 [K]**	**V_0 (m/s)**	**t (ms)**	**V_R (m/s)**
3.0	46	293	78.84	0.000	0.00	2.0	56A	423	65.27	0.000	0.00
3.5	47	293	85.62	1.680	29.76	2.5	56	423	72.05	1.860	26.88
4.0	48	293	90.25	1.200	41.67	3.0	57	423	78.37	1.116	44.80
5.0	49	293	100.00	0.780	64.10	4.0	58	423	90.25	0.810	61.73
7.5	50	293	120.77	0.570	87.72	5.0	59	423	100.00	0.670	74.63
						7.5	60	423	120.19	0.490	102.04
Ballistic limit estimation 82 m/s						Ballistic limit estimation 69 m/s					
Aluminium plates + 9 mm rubber											
Press. (bars)	**Test No**	**T_0 [K]**	**V_0 (m/s)**	**t (ms)**	**V_R (m/s)**	**Press. (bars)**	**Test No**	**T_0 [K]**	**V_0 (m/s)**	**t (ms)**	**V_R (m/s)**
2.5	61*	293	-	-	-	2.5	71A	423	71.60	0.000	0.00
3.0	62*	293	-	-	-	2.8	71	423	76.22	1.620	30.86
4.0	63	293	89.60	Project. stuck	0.00	3.5	72	423	86.51	0.960	52.08
4.6	63A	293	96.60	1.440	34.72	4.0	73	423	90.58	0.870	57.47
5.0	64	293	100.00	1.140	43.86	5.0	74	423	101.04	0.720	69.44
7.5	65	293	118.28	0.700	71.43	7.5	75	423	121.36	0.540	92.59
Ballistic limit estimation 93 m/s * no records						Ballistic limit estimation 74 m/s					

The estimation of the energy bulk dissipated during the perforation process is presented in Fig. 6. The values of the energy dissipated did not reveal any visible trend, they change as a function of the initial temperature of the experiment.

It is important to propose a reliable numerical model in order to reproduce experimental results and extend the analysis to the domain not covered by experiment. The estimation of the local temperatures and strain rates encountered during the perforation process will be given using a FE model.

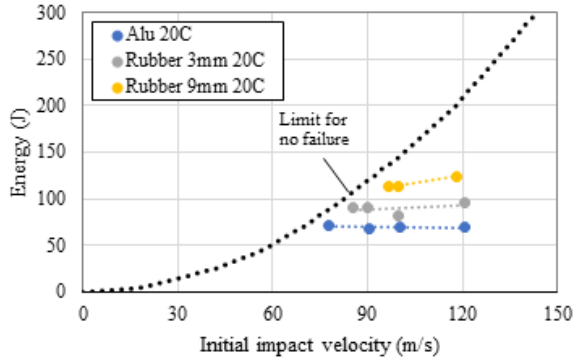

a)

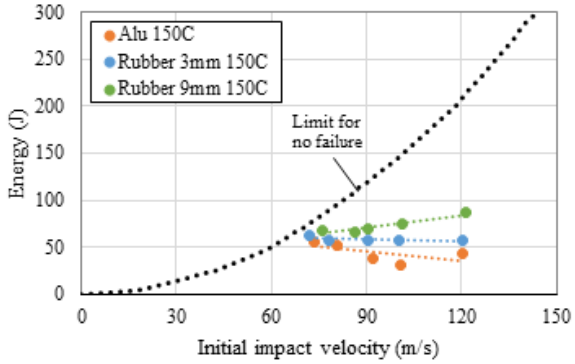

b)

Figure 6

Experimental results of energy absorbed by the specimen as a function of the initial impact velocity V_0 for different specimen configurations and temperatures (T_0=293 K/20˚C and T_0=423 K/150˚C); "limit for no failure" denotes a transition between perforation and non-perforation zones

4 Numerical Thermomechanical Model for Perforation

4.1 Initial and Boundary Conditions

Numerical calculations were performed using Abaqus/Explicit program dedicated for high rates of deformations in line with the practice used in previous works [33-34]. In all calculations, the aluminium-rubber composite and projectile were modelled as presented in Fig. 7. Aluminum plates were modelled as shell finite elements and the rubber as solid finite elements.

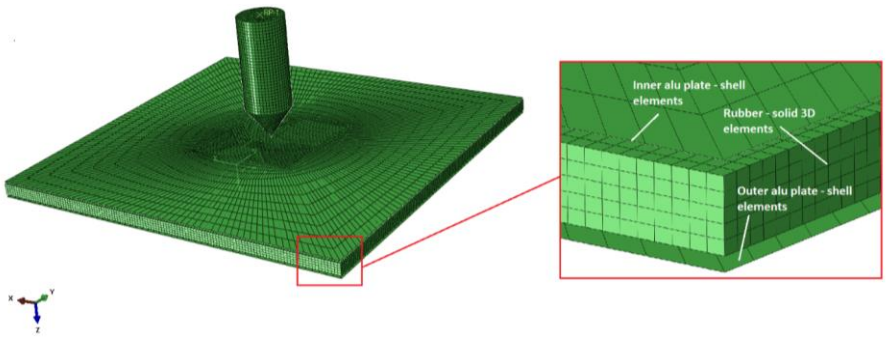

Figure 7
FE model of aluminium plates and rubber

During computer calculations the aluminium-rubber composites were fixed along the four sides of the specimen in order to model the boundary conditions used in the laboratory tests (full fixation).

The mesh size sensitivity were checked in the simulations. The failure patterns and the value of the residual velocity were compared for different meshes. Thanks to this analysis, the optimal mesh is used then in all further simulations of the perforation process. The following number of elements was used:

- for discretization of the specimen: fine mesh in the middle: 3570 nodes, 3450 elements type Shell S4R; remaining part: 2611 nodes, 2598 elements type Shell S4R; both parts of the specimen were tied in the analysis, the refined mesh part has a form of a circle 5 cm in diameter in the region of contact between the two acting bodies,
- for discretization of the rubber component:

  3 mm thickness case: 95256 nodes, 78125 elements type Solid (C3D8R, 5 elements along the thickness, average element dimensions is $8x10^{-5}$ mm x $8x10^{-5}$ mm x $8x10^{-5}$ mm),
- 9 mm thickness case: 254016 nodes, 234375 elements type Solid 185(8) (C3D8R. 15 elements along the thickness, average element dimensions is $8x10^{-5}$ mm x $8x10^{-5}$ mm x $8x10^{-5}$ mm),
- for discretization of the projectile: 10842 nodes, 9648 elements.

The friction between the projectile and the plate is an important parameter as discussed in [22, 35-37], it was assumed as constant and equal to 0.3 to reflect the friction observed between the bodies. The general contact was used together considering interior contact surfaces created during failure or erosion of the mesh related to the material. The friction rubber-metal is defined using the friction coefficient equal to 0.4.

The analysis was assumed as adiabatic. The adiabatic heat effect is defined using the heat equation without conductivity (k=0) and assuming a Quiney-Taylor coefficient as constant and equal to 0.9. The material parameters used are a specific heat C_p=900 J/kgK and a density ρ=2700 kg/m^3. The range of the initial temperatures T_0 reflect the experiment range, i.e., 293 K-423 K.

4.2 Material Modelling

The Johnson-Cook [38] constitutive hardening relation is used to describe the dynamic material behaviour of the aluminium plate:

$$\overline{\sigma}\left(\overline{\varepsilon}_{pl}, \dot{\overline{\varepsilon}}_{pl}, T\right) = \left(A + B\overline{\varepsilon}_{pl}{}^{n}\right)\left(1 + C ln\frac{\dot{\overline{\varepsilon}}_{pl}}{\dot{\varepsilon}_0}\right)\left[1 - \left(\frac{T - T_0}{T_m - T_0}\right)^m\right] \tag{3}$$

where A is the yield stress, B and n are the strain hardening exponent, C is the strain rate sensitivity coefficient, $\dot{\varepsilon}_0$ is strain rate reference value and m is the temperature sensitivity parameter. The last bracket in Eq. 3, describes the thermal softening of the material and reduces the limit of the Mises equivalent stress $\overline{\sigma}$ from the reference temperature T_0 to zero at melting temperature T_m.

The constants of Johnson-Cook constitutive model adopted for numerical simulations are given in Table 2. The basic constants A, B and n were deducted from our own testing results, whereas the temperature and strain rate effect were adopted from [22].

Table 2
Constants of Johnson-Cook model

A (MPa)	B (MPa)	n (-)	C (-)	m (-)	T_0 (K)	T_m (K)	$\dot{\varepsilon}_0$ (-)
104	90	0.40	0.01	1.8	293.15	933	1.0

Concerning the failure criterion, the equivalent plastic strain at failure $\varepsilon_{pl}^{f}(T)$ as a function of temperature was adopted, this damage initiation value changes linearly from 1.22 at T=293 K to 0.7 at T=603 K. The use of this simplified criterion was reported with success in [22, 24, 26, 37]. The parametrical analysis of the effective failure criterion consisted of observing the failure modes (petaling) and fitting the numerical ballistic curves to the experimental ones. The failure criterion applied in simulations eliminates the elements in which the critical value of the equivalent plastic strain ε_{pl}^{f} is reached.

The deformations of the middle layer of the perforated composite slabs are modelled by coupling the hyperelasticity with rate-dependent plasticity together with damage and failure of the material. The temperature softening is also considered since it affects the rubber behaviour [39]. From mathematical point of view, the model is using the multiplicative split of deformation gradient into elastic and plastic parts according to:

$$F = F_e \cdot F_p, \tag{4}$$

where F_e is the elastic part of the deformation gradient and it represents the hyperplastic behaviour and F_p is the plastic part of the deformation gradient (permanent). The incompressible isotropic hardening Mises plasticity with associated flow rule is used in the model together with hyperelasticity. In the current analysis the Marlow model is assumed [40]. The strain rates effect is included only in the plastic part of deformation. In the current analysis, the rate independent behaviour was assumed. The damage and failure is also imposed on the plastic part of the deformation gradient. In this analysis, the temperature sensitivity was additionally added to both the hyperelastic and plastic part of the deformations. The important fact is that the hyperalastic model should be defined by nominal stress versus nominal strain curve. Abaqus automatically identifies the parameters of the selected optimal model (Marlow model selected). The plasticity is defined by the true stress vs. true plastic strain curve. The constant value of 1.25 of the initiation damage plastic strain was assumed. The evolution of the damage was defined by the displacement at failure (0.01 mm). The energetic strain softening regularisation was used as it was for aluminium, 50% maximum degradation was allowed before the final failure at which the finite element was deleted from the mesh. The definition of the rubber is presented in Fig. 8 and Table 3.

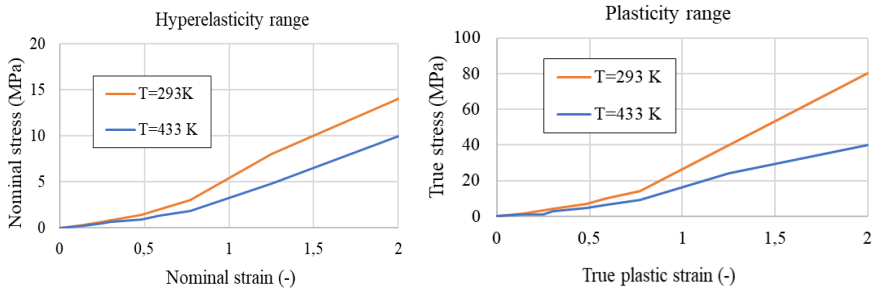

Figure 8
Rubber modelling – stress-strain curves for hypelastic and plastic ranges at different temperatures

Table 3
Rubber modelling – Abaqus command used for material definition

*Hyperelastic, Marlow, Poisson=0.5 *Uniaxial Test Data	*Plastic
*Damage Initiation, criterion=DUCTILE 1.25 *Damage Evolution, type=DISPLACEMENT 0.01 *Density 9.6e-10	

5 Results and Discussions

Numerical results are presented in Fig. 9. The model successfully reproduced the experimental behaviour presented in Fig. 5. Very similar petaling forms are given. In case of the internal plate (Fig. 9b), an extended form is produced with walls partially perpendicular to the specimen plane. The petaling is in a rather rugged form. Some 5-8 non-shaped petals are reported. Another form is observed in the outer specimen – 3-4 typical petals as usually seen in aluminium only studies [21, 41].

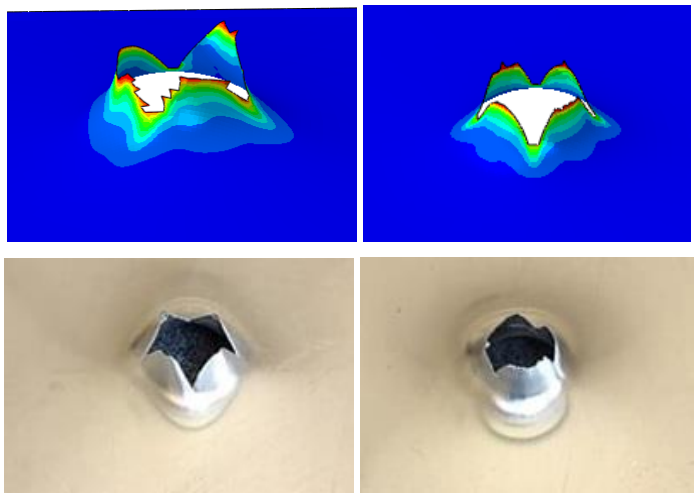

a) b)

Figure 9
View of the perforation forms in metal specimens – numerical simulation vs. experiment, a) inner plate (impacted first), b) outer plate

The numerical simulations permitted to estimate the mean temperature increase during the adiabatic heating in petals: configuration 1 (aluminium only) - $\Delta T = 66$ K, configurations 2 and 3 (aluminium-rubber composite) - $\Delta T = 54$ K. The mean strain rates values in petals developed during impact were the following: configuration 1 (aluminium only) - $\dot{\varepsilon} = 9.1 \cdot 10^3$ 1/s, configurations 2 and 3 (aluminium-rubber composite) - $\dot{\varepsilon} = 5.4 \cdot 10^3$ 1/s. No temperature increase was measured in rubber. In both cases, i.e., in numerical calculations and experimental tests, the same characteristic petals in the region of perforation are observed, which confirms the accuracy of the constitutive law and failure criterion used.

Figure 10 presents comparison of the material response obtained from analytical, experimental and numerical studies. The results presented in the form of the initial impact velocity V_0 vs. residual velocity V_R have shown the numerical values overlap with the experimental ones. The numerical findings are close to Ipson-Recht analytical approach [21] and experiments. The Ipson-Recht coefficient κ was slightly changing across the analysis as shown in Table 4.

Table 4

The Ipson-Recht coefficient κ

□	Configuration 1: 2 aluminium plates	Configuration 2: aluminium-3 mm rubber-aluminum	Configuration 3: aluminium-9 mm rubber-aluminum
T_0=293 K	2.0	1.75	2.2
T_0=423 K	2.5	2.2	2.0

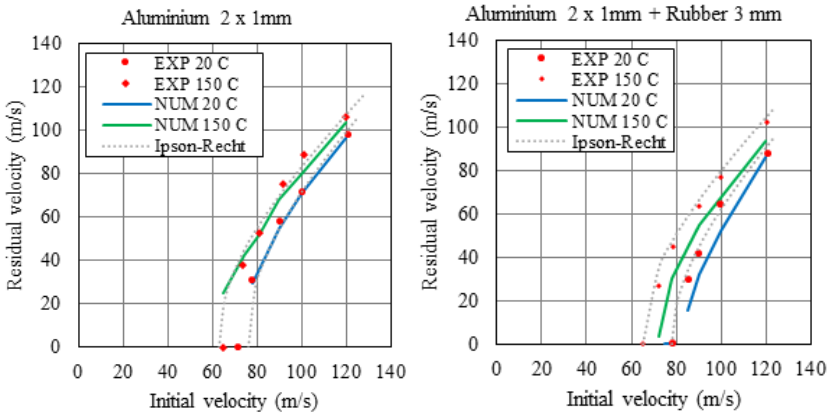

a) b)

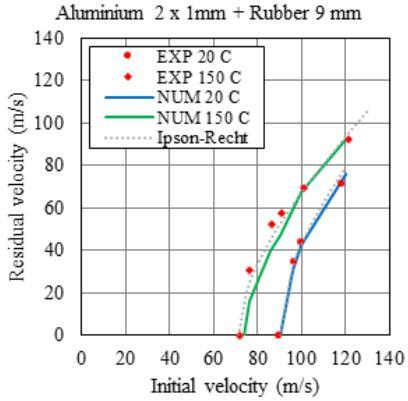

c)

Figure 10
Initial impact velocity V_0 vs. residual velocity V_R – analytical vs. experimental vs. numerical results, a) config. 1, T_0=273 K/423 K, b) config. 2, T_0=273 K/=423 K, c) config. 3, T_0=273 K/423 K

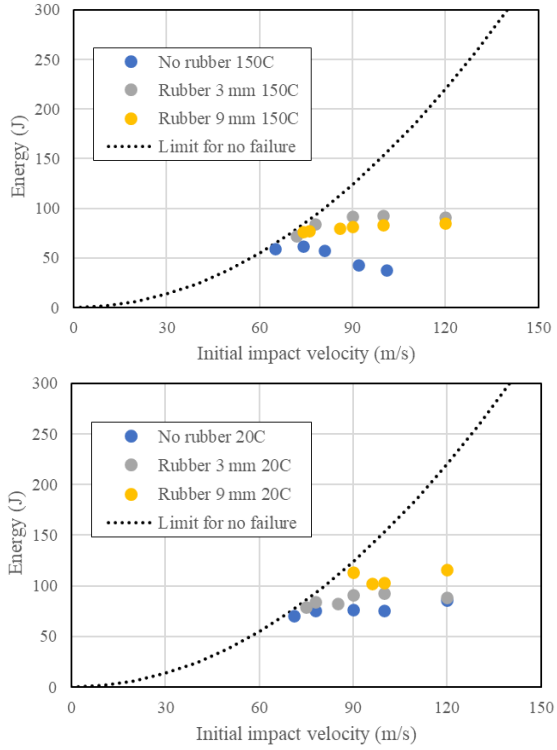

Figure 11
Numerical simulations results of energy absorbed by the specimen as a function of the initial impact velocity V_0 for different specimen configurations and temperatures (T_0=293 K/20˚C and T_0=423 K/150˚C); “limit for no failure” denotes a transition between perforation and non-perforation zones

In Figure 11 numerical simulations results of energy absorbed by the specimen as a function of the initial impact velocity V_0 can be found. The values are given for two different temperatures (T_0=293 K and T_0=423 K) and for all specimens configurations. Close similarities of results are found when compared with Figure 6 where the energy values are given for the same test conditions but in real experiment.

The experimental records concerning the reaction force is given in Fig. 12. The preliminary tests were performed at one temperature of 293 K and one initial impact velocity V_0~90 m/s. The aim of that extra study consisted of checking the effect of the sandwich configuration on the force exerted during perforation. The general observation was that the reaction force diminished with the rubber thickness increase. As discussed in [42], the value of the experimentally determined reaction force may be obscured by the inertia of the system that impacts the measurements. A complex numerical model would be then required for better reaction force estimation. Different approaches to estimate reaction forces may be used in the numeric model: summing up nodal values in fixation points, using the acceleration history of the projectile or by building up a complex FE model including heavy metal support and 3D sensor geometries.

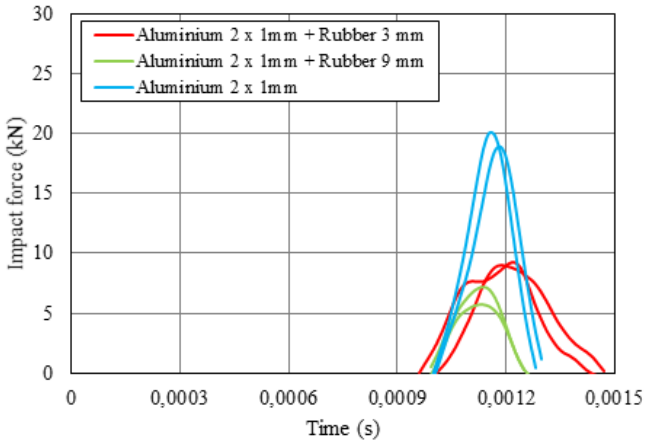

Figure 12

Reaction force measured during experiment for 3 composite configurations (ambient temperature, V_0~90 m/s)

Conclusions

The paper presents results of experimental tests and numerical simulations by FE method carried out on the aluminium-rubber composite. The composite specimens were tested under perforation regime within a wide range of impact velocities V_0 and initial temperatures T_0. The aim of the study was to analyze different configurations of the composite, especially in terms of the thickness of the rubber component. The increase of the rubber layer increased the ballistic limit.

Conversely, the temperature diminished the ballistic properties of the rubber composite: it lowered the ballistic limit as both aluminium and rubber softened. The maximum analysed temperature (T=423 K) is close to the melting point of rubber (T_m~453 K) and its impact on the ballistic resistance at these temperature conditions was observed both in experiment and simulations. An interesting observation concerned the measurements of the reaction force: the increasing of the rubber thickness resulted in decreasing of the reaction force.

The implemented Johnson-Cook constitutive relation in the FE analysis combined with the proposed effective failure criterion allowed reproduction of experimental findings in terms of the ballistic limit and failure modes. The model allowed us to estimate the local maxima of the adiabatic temperature increase (ΔT = 54-66 K) and local maxima of strain rate recorded during perforation ($\dot{\varepsilon}$ = 5.4-9.1·10^3 1/s).

The typical failure mode of the aluminium plates was observed during the tests with the same number of 3 or 4 petals in the outer plate and 5-8 petals in the inner one. A good correlation between the results calculated by FEM method and those obtained from experiments is observed. The shape of petaling was different for internal and external aluminium plates. Concerning the rubber, one or two cracks remained after the projectile passage, but with no plastic deformation of the material, which reflected the hyperelastic nature of the material.

Acknowledgments

The support of Richard Bernier from University of Lorraine, Laboratory of Microstructure Studies and Mechanics of Materials LEM3 during the perforation tests in Metz is highly acknowledged.

References

[1] G. Tiwari, M. Iqbal, P. Gupta, Energy absorption characteristics of thin aluminium plate against hemispherical nosed projectile impact, Thin-Walled Struct. 126 (2018) 246-257

[2] Z. Rosenberg, R. Kositski, E. Dekel, On the perforation of aluminum plates by 7.62 mm APM2 projectiles, Int. J. Impact Eng. 97 (2016) 79-86

[3] M. Iqbal, S. Khan, R. Ansari, N. Gupta, Experimental and numerical studies of double-nosed projectile impact on aluminum plates, Int. J. Impact Eng. 54 (2013) 232-245

[4] M. Rodriguez-Millan, D. Garcia-Gonzalez, A. Rusinek, F. Abed, A. Arias, Perforation mechanics of 2024 aluminium protective plates subjected to impact by different nose shapes of projectiles, Thin-Walled Struct. 123 (2018) 1-10

[5] K. Senthil, M. Iqbal, B. Arindam, R. Mittal, N. Gupta, Ballistic resistance of 2024 aluminium plates against hemispherical, sphere and blunt nose projectiles, Thin- Walled Struct. 126 (2018) 94-105. [6] K. Ackland, C.

Anderson, T. D. Ngo, Deformation of polyurea-coated steel plates under localised blast loading, Int. J. Impact Eng. 51 (2013) 13-22

[6] Alavi Nia A, Hoseini GR. Experimental study of perforation of multi-layered targets by hemispherical-nosed projectiles. Materials & Design 2011;32:1057-65

[7] Rodríguez-Martínez JA, Rusinek A, Arias A. Thermo-viscoplastic behaviour of 2024-T3 aluminium sheets subjected to low velocity perforation at different temperatures. Thin-Walled Structures 2011;49:819-32

[8] Rusinek A, Bernier R, Boumbimba RM, Klosak M, Jankowiak T, Voyiadjis GZ. New devices to capture the temperature effect under dynamic compression and impact perforation of polymers, application to PMMA. Polymer Testing 2018;65:1-9

[9] Klosak M, Rusinek A, Bendarma A, Jankowiak T, Lodygowski T, Klosak M, et al. Experimental study of brass properties through perforation tests using a thermal chamber for elevated temperatures. Latin American Journal of Solids and Structures 2018;15

[10] Jia, B., Rusinek, A., Bahi, S., Pesci, R., Bendarma, A. Perforation Behavior of 304 Stainless Steel Plates at Various Temperatures, Journal of Dynamic Behavior of Materials, 2019, 5(4), pp. 416-431

[11] K. Ackland, C. Anderson, T. D. Ngo, Deformation of polyurea-coated steel plates under localised blast loading, Int. J. Impact Eng. 51 (2013) 13-22

[12] R. Gamache, C. Giller, G. Montella, D. Fragiadakis, C. Roland, Elastomer-metal laminate armor, Mater. Des. 111 (2016) 362-368

[13] I. Mohagheghian, G. J. McShane, W. Stronge, Quasi-static and impact perforation of polymer-metal bi-layer plates by a blunt indenter, Thin-Walled Struct. 117 (2017) 35-48

[14] Y. Dong, Y. Ke, Z. Zheng, H. Yang, X. Yao, Effect of stress relaxation on sealing performance of the fabric rubber seal, Compos. Sci. Technol. 151 (2017) 291-301

[15] H. Yang, X.-F. Yao, Y.-C. Ke, Y.-j. Ma, Y.-H. Liu, Constitutive behaviors and mechanical characterizations of fabric reinforced rubber composites, Compos. Struct. 152 (2016) 117-123

[16] H. Yang, X.-F. Yao, H. Yan, Y.-n. Yuan, Y.-F. Dong, Y.-H. Liu, Anisotropic hyper- viscoelastic behaviors of fabric reinforced rubber composites, Compos. Struct. 187 (2018) 116-121

[17] A. Khodadadi, G. Liaghat, H. Ahmadi, A. R. Bahramian, O. Razmkhah, Impact response of Kevlar/rubber composite, Compos. Sci. Technol. 184 (2019) 107880

[18] P. Zhang, X. Kong, Z. Wang, C. Zheng, H. Liu, G. Shi, J. P. Dear, W. Wu, High velocity projectile impact of a composite rubber/aluminium fluid-filled container, International Journal of Lightweight Materials and Manufacture 4 (2021) 1-8

[19] D. Rajkumar, V. Mahesh, S. Joladarashi, S. M. Kulkarni, Parametric study on impact behaviour of sisal and cenosphere reinforced natural rubber-based hybrid composites: FE approach, Materials Today: Proceedings, vol. 46 (17), 8767-8771, 2021

[20] Z. Huanga, L. Suia, F. Wanga, S. Dub, Y. Zhoua, J. Ye, Dynamic compressive behavior of a novel ultra-lightweight cement composite incorporated with rubber powder, Composite Structures 244 (2020) 112300

[21] R. F. Recht and T. W.Ipson, Ballistic perforation dynamics, Journal of Applied Mechanics, 30, 3, pp. 384-390, 1963

[22] A. Bendarma, T. Jankowiak, T. Łodygowski, A. Rusinek and M. Klosak, Experimental and numerical analysis of the aluminum alloy AW5005 behaviour subjected to tension and perforation under dynamic loading, Journal of Theoretical and Applied Mechanics, 55, 4, pp. 1219-1233, 2016

[23] M. Klosak, T. Jankowiak, A. Rusinek, A. Bendarma, P. W. Sielicki and T. Lodygowski, Mechanical Properties of Brass under Impact and Perforation Tests for a Wide Range of Temperatures: Experimental and Numerical Approach, Materials, 13, 24, 5821, 2020

[24] A. Bendarma, T. Jankowiak, A. Rusinek, T. Lodygowski, M. Klosak, Perforation Tests of Aluminum Alloy Specimens for a Wide Range of Temperatures Using High-Performance Thermal Chamber-Experimental and Numerical Analysis, In IOP Conference Series: Materials Science and Engineering, IOP Publishing, 491, 1, 012027, 2019

[25] A. Bendarma, H. Gourgue, T. Jankowiak, A. Rusinek, S. Kardellass, M. Klosak, Perforation tests of composite structure specimens at wide range of temperatures and strain rates-experimental analysis, Materials Today: Proceedings, 24, 7-10, 2020

[26] A. Bendarma, A. Rusinek, T. Jankowiak, T. Lodygowski, B. Jia, Experimental analysis of the aluminum alloy sheet subjected to impact and perforation process, Materials Today: Proceedings, 36, 88-93 2021.[

[27] D. Garcia-Gonzalez, A. Rusinek, A. Bendarma, R. Bernier, M. Klosak, S. Bahi, Material and structural behaviour of PMMA from low temperatures to over the glass transition: Quasi-static and dynamic loading, Polymer Testing, 81, 106263, 2020

[28] T. Jankowiak, A. Rusinek, K.M. Kpenyigba and R. Pesci, Ballistic behaviour of steel sheet subjected to impact and perforation, Steel and Composite Structures, 16, 6, pp. 595-609, 2014

[29] A. Rusinek, J. A. Rodrıguez-Martınez, R. Zaera, J. R. Klepaczko, A. Arias and C. Sauvelet, Experimental and numerical study on the perforation process of mild steel sheets subjected to perpendicular impact by hemispherical projectiles, International Journal of Impact Engineering, 36, 4, pp. 565-587, 2009

[30] T. Børvik, O, S. Hopperstad, M. Langseth and K. A. Malo, Effect of target thickness in blunt projectile penetration of Weldox 460 E steel plates, International Journal of Impact Engineering, 28, 4, pp. 413-464, 2003

[31] B. Landkof and W. Goldsmith, Petaling of thin metallic plates during penetration by cylindro-conical projectiles, International Journal of Solids and Structures, 21, 3, pp. 245–266, 1985

[32] K. M. Kpenyigba, T. Jankowiak, A. Rusinek and R. Pesci, Influence of projectile shape on dynamic behaviour of steel sheet subjected to impact and perforation, Thin-Walled Structures, 65, pp. 93-104, 2013

[33] T. Jankowiak, A. Rusinek and P. Wood, A numerical analysis of the dynamic behaviour of sheet steel perforated by a conical projectile under ballistic conditions, Finite Elements in Analysis and Design, 65, pp. 39-49, 2013

[34] A. Arias, J. A. Rodríguez-Martínez and A. Rusinek, Numerical simulations of impact behaviour of thin steel plates subjected to cylindrical, conical and hemispherical non-deformable projectiles, Engineering Fracture Mechanics, 75, pp. 1635-1656, 2008

[35] A. Massaq, A. Rusinek, M. Klosak, F. Abed and M. El Mansori, A study of friction between composite-steel surfaces at high impact velocities, Tribology International, 102, pp. 38-43, 2016

[36] Z. Rosenberg and Y. Vayig, On the friction effect in the perforation of metallic plates by rigid projectiles, International Journal of Impact Engineering, 149, 103794, 2021

[37] A. Bendarma, T. Jankowiak, A. Rusinek, T. Lodygowski, B. Jia, M. H. Miguélez, M. Klosak, Dynamic Behavior of Aluminum Alloy Aw 5005 Undergoing Interfacial Friction and Specimen Configuration in Split Hopkinson Pressure Bar System at High Strain Rates and Temperatures. Materials, 13(20), 4614, 2020

[38] G. R. Johnson and W. H. Cook, A constitutive model and data for metals subjected to large strains, high strain rates and high temperatures, in Proceedings of the 7th International Symposium on Ballistics, 21, pp. 541-547, 1983

[39] G. Weber, L. Anand, Finite Deformation Constitutive Equations and Time Integration Procedure for Isotropic Hyperelastic-Viscoplastic Solids, Computer Methods in Applied Mechanics and Engineering, 79, 173-202, 1990

[40] A. Aidy, M. Hosseini, B. B. Sahari, A Review of Constitutive Models for Rubber-Like Materials, American Journal of Engineering and Applied Sciences, 3 (1), 232-239, 2010

[41] W. Mocko, J. Janiszewski, J. Radziejewska and M. Grazka, Analysis of deformation history and damage initiation for 6082-T6 aluminium alloy loaded at classic and symmetric Taylor impact test conditions, International Journal of Impact Engineering, 75, pp. 203-213, 2015

[42] W. Z. Zhong, A. Mbarek, A. Rusinek, R. Bernier, T. Jankowiak and G. Sutter, Development of an experimental set-up for dynamic force measurements during impact and perforation, coupling to numerical simulations, International Journal of Impact Engineering, 91, pp. 102-114, 2016